

Star formation in bar environments

I. Morphology, star formation rates and general properties

P. Martin¹ and D. Friedli^{2,3}

¹ European Southern Observatory, Casilla 19001, Santiago 19, Chile (e-mail: pmartin@sc.eso.org)

² Département de physique and OMM, Université Laval, Ste-Foy, Québec, G1K 7P4, Canada (e-mail: dfriedli@phy.ulaval.ca)

³ Geneva Observatory, CH-1290 Sauverny, Switzerland

Received 19 March 1997 / Accepted 5 May 1997

Abstract. A study of the morphological properties and star formation rates (SFRs) of H II regions located along the bars of a sample of eleven late-type barred systems is presented and compared with numerical simulations. According to the relative intensity of star formation along the bar with respect to that of the nuclear region, three types of distributions are observed. They may be related to the age of the bar. Other important characteristics include angular misalignments (up to 15°) between the stellar bar and the “H α bar”, a correlation between the location of the H II regions and dust lanes in certain bars (mostly early-type spirals), and a difference in axial ratio and length between stellar and H α bars. A wide range of SFRs (from 0.03 to $1.44 M_\odot \text{ yr}^{-1}$) is observed, and star formation is generally highly asymmetric with respect to the bar minor axis. All these features can be reproduced in numerical models provided that the global mechanical energy release remains low (but non-zero). In NGC 7479, the total gas-to-star transformation efficiency inside the bar is estimated at about 0.26, meaning that, at present, maybe as nearly as 75% of the gas flowing into the bar region is not transformed into stars.

Key words: galaxies: evolution – galaxies: ism – galaxies: kinematics and dynamics – galaxies: spiral – galaxies: structure

1. Introduction

Bars are present in a large fraction of spiral galaxies and can trigger a rich variety of phenomena (for recent reviews see Sellwood & Wilkinson 1993; Martinet 1995). Numerous numerical simulations (e.g. Roberts et al. 1979; Combes & Gérin 1985; Noguchi 1988; Athanassoula 1992, 1994; Wada & Habe 1992, 1995; Friedli & Benz 1993, 1995; Friedli et al. 1994; Heller & Shlosman 1994; Piner et al. 1995; Laine 1996; Englmaier & Gerhard 1997) and observations (e.g. Ball 1986; Ondrechen &

van der Hulst 1989; England et al. 1990; Jörsäter & van Moorsel 1995; Moore & Gottesman 1995; Lindblad et al. 1996) have revealed that non-axisymmetric features like bars induce large-scale gas flows inside them as well as across the discs of parent galaxies. The importance of these flows for galaxy evolution is clearly seen, for instance, in the radial distribution of O/H abundances in barred galaxies: O/H gradients in barred spirals are significantly shallower than those in normal spirals. This behaviour is the result of large-scale mixing of chemical elements after a few galactic rotations (Martin & Roy 1994, 1995; Friedli et al. 1994; Friedli & Benz 1995; Roy 1996). Despite progress made in understanding bar influence on chemical evolution, the role played by gas flows on *large-scale star formation* (SF) and fueling AGN and nuclear starbursts remains unclear in barred galaxies.

As reviewed by Kennicutt (1994), the effects of radial gas flows triggered by bars on SF distributions across spirals are more difficult to identify for several reasons: 1) the data available are still sparse and it is difficult to separate bar-triggered phenomena from those which are manifestations of the normal SF process; 2) star formation properties of barred galaxies vary a lot; 3) we lack of a good theory for large-scale SF in galaxies. In particular, bars have been found either to enhance SF (e.g. Hawarden et al. 1986; Arsenault 1989), or not to enhance SF (e.g. Pompea & Rieke 1990; Isobe & Feigelson 1992). Using available data on integrated H α photometry of disc galaxies Kennicutt (1994) has shown that there seems to be no detectable difference between the *global* star formation rates (SFRs) of barred and normal spirals. However, amongst a sample of isolated late-type galaxies, Martinet & Friedli (1997) have found that all the most active star forming galaxies host a *strong* bar (see also Martin 1995; Contini 1996). In any case, a close examination of an atlas of galaxies reveals that barred spirals have some unique SF properties, particularly in the inner parts of their discs. For example, star forming regions along the bar (e.g. NGC 3359, NGC 7479), a bar completely devoid of H II regions (e.g. NGC 4303), a circumnuclear ring of H II regions or “hotspots” (e.g. NGC 1300), an enhancement of SF activity at the ends

Send offprint requests to: P. Martin

of the bar (e.g. M83, NGC 1300) or a ring around the bar (e.g. NGC 1512) are the most frequently observed morphologies (see García-Barreto et al. 1996 for other examples).

This diversity was recently reviewed by Phillips (1996) who explored quantitatively these different distributions of H II regions in barred spirals and also studied their luminosity functions (LF). He found a clear difference in SF activity between early-type and late-type systems, the latter frequently showing bright H II regions along their bars contrary to the former. Possible differences between the H II region LFs also appear but a definitive conclusion seems difficult to draw because crowding of H II regions in bars affects such a study. Unfortunately, the images used in the present study have an average seeing of 1.2'' to 1.5'' and do not allow us to investigate this important problem. According to García-Barreto et al. (1996), SF along bars appears indeed quite frequent in late-type systems (25% of their sample of 52 galaxies in comparison to 10% for the early-type galaxies). The same morphology is seen also in a few barred spirals of the Virgo cluster (Koopman et al. 1996). Martin & Roy (1995) and Friedli & Benz (1995, hereafter FB95) have argued that the presence of SF activity along bars could indicate that these structures are young ($\lesssim 1$ Gyr), in a phase where large amounts of gas are shocked and funnelled along their major axes. Using the O/H distribution in its disc, Martin & Roy (1995) have estimated the age of the bar in NGC 3359, which shows several H II regions, to be about 400 Myr, in good agreement with the scenario of recently formed bar.

In this study, presented as a series of three papers, we will focus on the morphology and physical properties of H II regions found along the bars of a sample of barred systems. We will address specific questions: 1) why is there such a variety in the amplitude of SF activity along galactic bars? 2) What is the exact distribution of H II regions in bars and how is it related to the dynamical properties of the host galaxy? 3) What is the duration of SF along bars? 4) What fraction of the gas funnelled along the bars is transformed into stars? 5) Are the physical properties (SFR, excitation, density, etc.) of H II regions in bars special?

The presence of SF along galactic bars offers a good opportunity to study SF processes taking place in environments where gas dynamics are strongly perturbed. It could also provide crucial clues to mechanisms operating during gas fueling of nuclear starbursts or AGN. In order to answer the above questions, we will use optical observations to derive the properties of SF activity along bars and carefully compare them with self-consistent 3D numerical simulations of bar formation including stars, gas, star formation, and radiative cooling.

In this paper we present H α observations of H II regions located in bars for two early-type and nine late-type barred galaxies. The sample, observations and data analysis are presented in Sect. 2. In Sect. 3, the general morphological properties of these H α bars are established and each galaxy of our sample is discussed individually. Star formation rates are derived in Sect. 4. Finally, a comparison with numerical models is presented in Sect. 5 whereas our conclusions are presented in Sect. 6. In Paper II (Martin 1997, in preparation), physical properties like O/H abundances, electronic density and excitation in a sub-sample

of H II regions observed in the bars of the galaxies studied here will be derived from long-slit spectroscopy data. A larger and more detailed set of numerical models will be presented in Paper III (Friedli & Martin 1997, in preparation).

2. Database

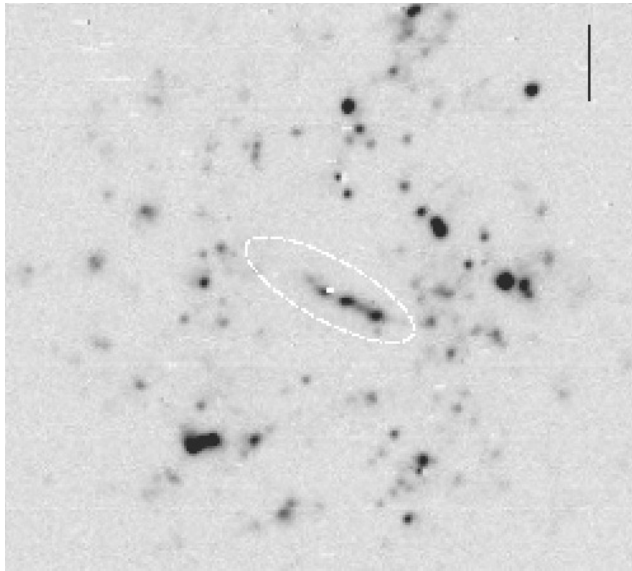
2.1. The sample of galaxies

Star formation activity along bars is not always easy to detect on normal photographic plates since the stellar continuum (frequently over-exposed) is usually much brighter than the H II regions. However, the colour atlas of Wray (1988) is a good place to start since the contrast is significantly improved by the tri-chrome technique. The galaxies included in our sample were all selected from this atlas. The selection was based on several astronomical and technical criteria: *i*) objects with apparently different amplitudes and distributions of SF activity in their bars were selected; *ii*) all the objects had to be at low redshifts (< 2400 km s $^{-1}$) due to the limited set of narrow-band H α filters available, and the need for resolving SF details along the bars; *iii*) since there is a clear difference in the SF activity between bars of early-type spirals and bars of late-type ones (Phillips 1996), a few early-types have been included in our sample; and *iv*) we have selected a few galaxies for which the H I (and sometimes CO) distributions were known.

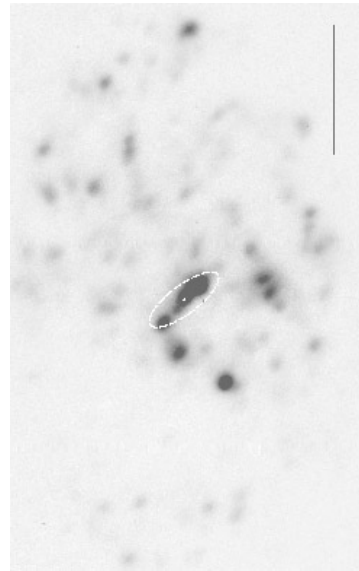
The general properties of the sample of galaxies are presented in Table 1. Adopted distances are from Tully (1988), and assume $H_0 = 75$ km s $^{-1}$ Mpc $^{-1}$. Only two galaxies show some activity in their nuclei, NGC 5921 and NGC 7479 (both LINERs).

2.2. Observations

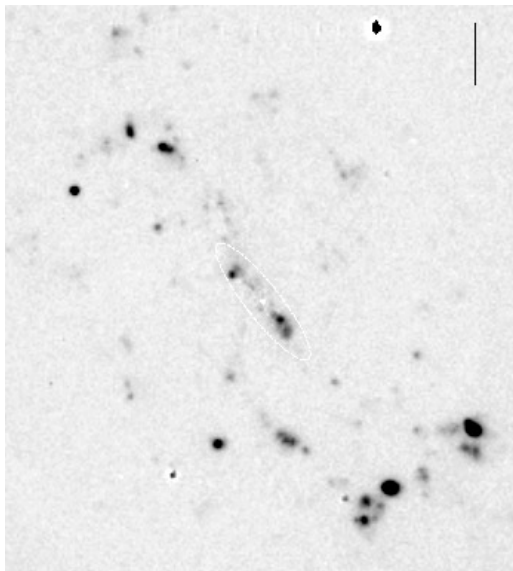
The H α observations were carried out with three different telescopes employed in four different configurations: the Mont Mégantic 1.6m telescope equipped with a focal reducer (f/3.5) and two different CCDs (RCA 320 \times 512 and Thomson 1k \times 1k); the Steward Observatory Bok 2.3m telescope (f/8) with a direct imager and an 800 \times 1200 Loral CCD, and the 0.9m telescope on Kitt Peak equipped with a 400 \times 400 TI CCD. The latter was used by R. Kennicutt to image NGC 3319. For each object the H α images were obtained with a narrow-band filter (carefully tuned to the redshift for the filters with $\Delta\lambda = 10$ Å) and another "off-band" filter was used to derive the contribution of the stellar continuum. A standard spectrophotometric star was observed for each object to calibrate the H α fluxes. Conditions were photometric in all cases. For observations conducted with the 2.3m telescope, most of the galaxies were not completely covered by the field of view (2.2' \times 2.2'). When possible, multiple exposures were performed. Observations for NGC 5068 were carried out when the object was low on the horizon (air-mass ~ 2) so the image presented here is not of the highest quality. The observing log is summarized in Table 2.



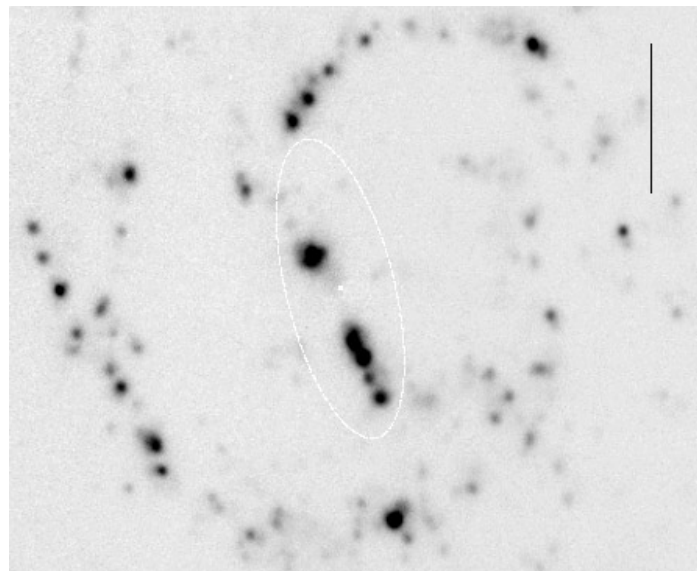
N1073



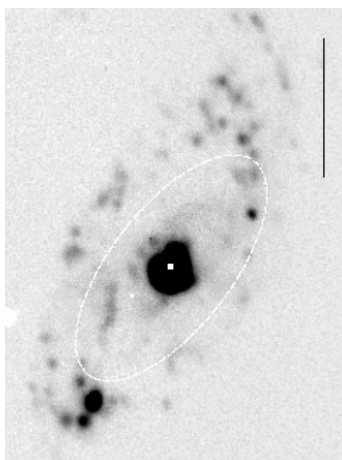
N1087



N3319

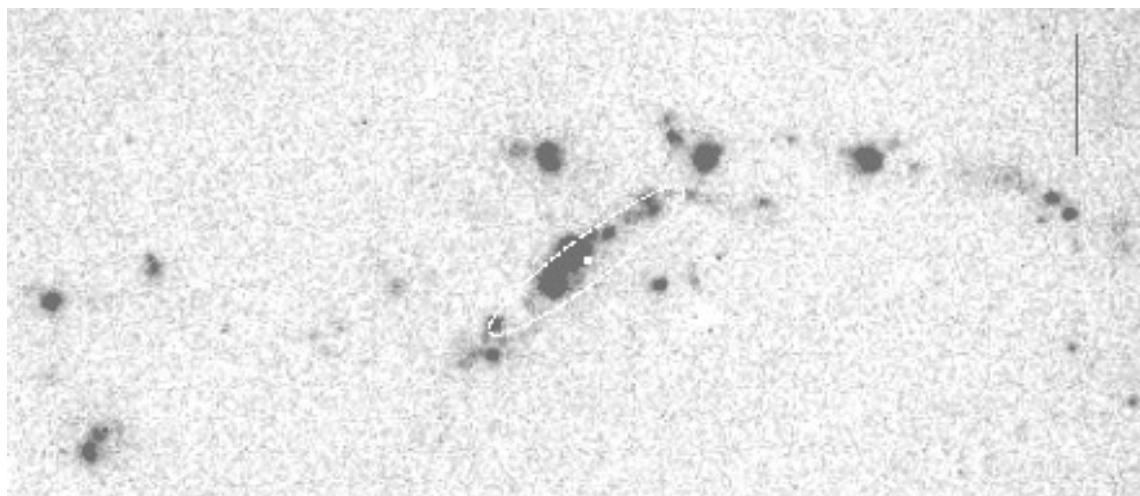


N3359

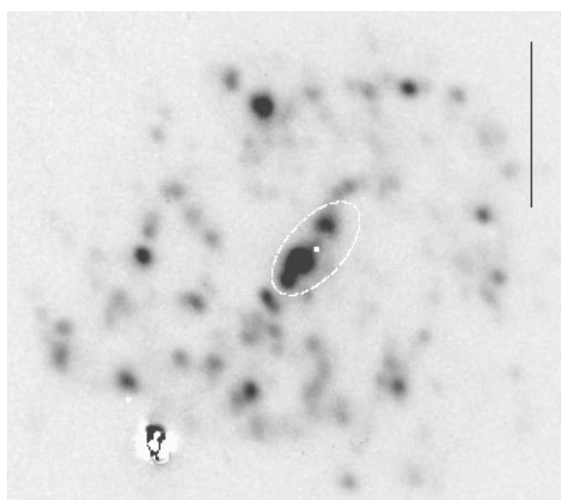


N3504

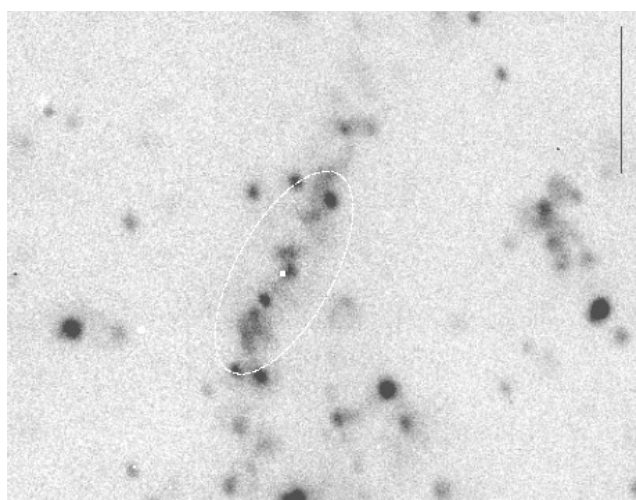
Fig. 1a–k. $H\alpha$ images of our sample barred spirals. The galaxy centres are indicated by a white dot. The stellar bars are represented by the ellipses indicating their position angles and axial properties. The vertical lines in the upper right corners correspond to the linear scale for $30''$. For all these images, North is at the top and East is to the left. **a** NGC 1073; **b** NGC 1087; **c** NGC 3319; **d** NGC 3359; **e** NGC 3504; **f** NGC 4731; **g** NGC 4900; **h** NGC 5068; **i** NGC 5921; **j** NGC 7479; **k** NGC 7741



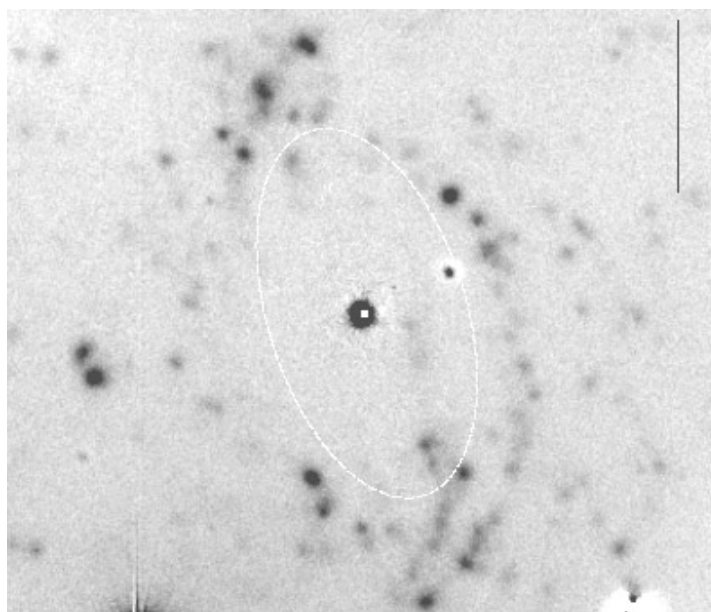
N4731



N4900

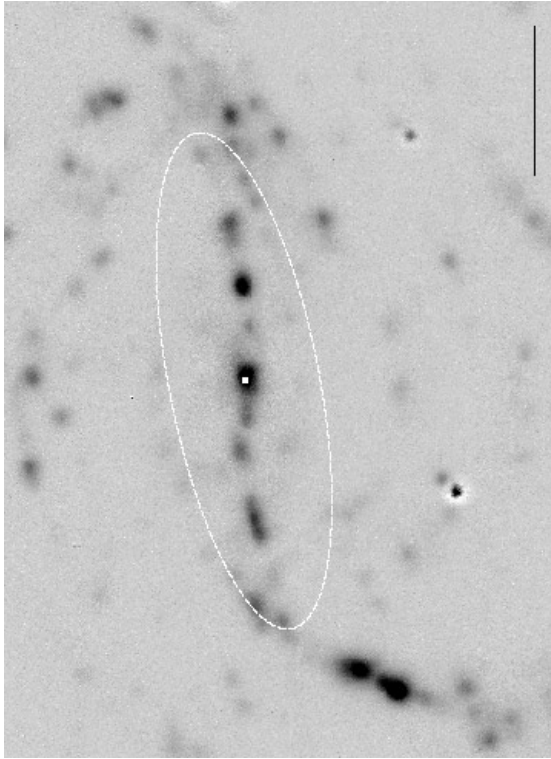


N5068

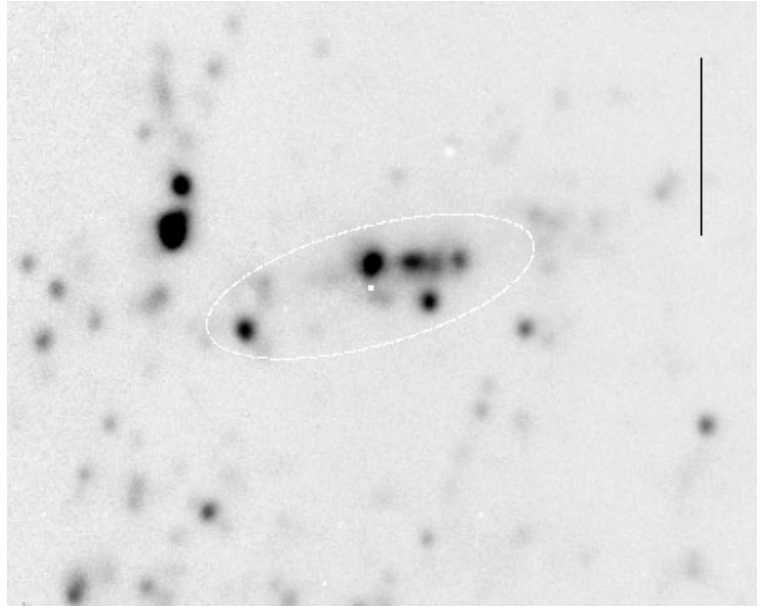


N5921

Fig. 1a-k. Continued



N7479



N7741

Fig. 1a–k. Continued

Table 1. The sample of galaxies

Galaxy	Type ^a	i^b [°]	PA ^a [°]	D_{25}^a [arcsec]	A_B^b [mag]	D^b [Mpc]	V^a [km s ⁻¹]	Scale [pc arcsec ⁻¹]
NGC 1073	SB(rs)c	24	165	294	0.08	15.2	1211	73.8
NGC 1087	SAB(rs)c	63	5	224	0.11	19.0	1519	92.2
NGC 3319	SB(rs)cd	57	37	370	0.00	11.5	742	55.8
NGC 3359	SB(rs)c	55	170	436	0.00	19.2	1013	93.2
NGC 3504	RSAB(s)ab	35	149	162	0.01	26.5	1539	128.6
NGC 4731	SB(s)cd	67	85	396	0.05	25.9	1495	125.7
NGC 4900	SB(rs)c	18 ^c	0 ^c	134	0.00	17.3	969	84.0
NGC 5068	SAB(rs)cd	29	110	436	0.32	6.7	673	32.5
NGC 5921	SB(r)bc	32	130	294	0.01	25.2	1480	122.3
NGC 7479	SB(s)c	45	25	244	0.16	32.4	2382	157.3
NGC 7741	SB(s)cd	51	170	262	0.12	12.3	749	59.7

References: ^a de Vaucouleurs et al. (1991); ^b Tully (1988); ^c Warmels (1988).

Table 2. Journal of observations

Galaxy	Epoch	Telescope	Scale [arcsec px ⁻¹]	H α Filter	Exposure [s]
NGC 1073	1988 Nov 4	1.6m	1.10	6602/10	3 × 2000
NGC 1087	1993 Oct 13	2.3m	0.30	6630/70	3 × 900
NGC 3319	1990 Feb 20	0.9m	1.25	6580/70	1 × 900
NGC 3359	1993 May 18	2.3m	0.30	6580/70	3 × 600
NGC 3504	1993 May 18	2.3m	0.30	6580/70	3 × 600
NGC 4731	1992 June 3	1.6m	0.70	6602/10	3 × 1500
NGC 4900	1993 May 18	2.3m	0.30	6580/70	3 × 600
NGC 5068	1993 May 18	2.3m	0.30	6580/70	1 × 380
NGC 5921	1993 May 17	2.3m	0.30	6580/70	3 × 600
NGC 7479	1993 June 18	2.3m	0.30	6630/70	3 × 600
NGC 7741	1993 May 18	2.3m	0.30	6580/70	3 × 800

2.3. Image analysis

Images were reduced following standard procedures. Biases were subtracted and flat-fielding was achieved by dividing the images by normalized high S/N dome flats. Large-scale residual illumination patterns were reduced to about 2% across the CCD fields. Sky background was measured in windows far from the galactic continuum and subtracted as a constant. The next step of the procedure, subtraction of the galactic continuum, is particularly critical for our study since it is most susceptible to affect the inner parts of the galaxy discs. To achieve the most accurate subtraction possible, the H α and continuum images were first superimposed very precisely (0.1 px) using several background stars. Afterwards, integrated fluxes of several field stars (> 5) were measured on the images and a first-order scaling factor was calculated. Many trial subtractions (~ 10) were then performed with slightly different factors in order to estimate how the first-order scaling factor measured from stars should be modified. Sky background, spiral arms and nuclear regions were carefully examined to look for artifacts caused by the subtraction procedure (e.g. holes or humps). Finally, fine-tuning of the best scaling factor found was performed by changing the value by a few percent in steps of 1% or less. Integrated fluxes of the H II regions were measured using circular windows the sizes of which matched the angular dimension of the regions. Flux calibration from standard stars was achieved using the filter transmission curves following the method described by Martin (1992) and Martin & Roy (1992).

The resulting H α images are presented for all the galaxies in our sample in Fig. 1. For each object, the extent, position angle and axial ratio of the *stellar bar* are indicated by an ellipse (see Sect. 3). The vertical lines in the upper right corners of these figures represent 30". The precision on the NS orientation is estimated to be about $\pm 2^\circ$.

3. Morphology

3.1. General distributions

The distribution of H II regions in the inner parts of galactic discs can be very complicated, particularly in the central regions (Keel 1983; Pogge 1989). However, although the H II regions are usually distributed non-uniformly in galactic bars as one can see from Fig. 1, their distributions can be adequately classified under three general types as already suggested by Martin & Roy (1995) (see also Sect. 4.2):

Type A. A “chain” of bright H II regions defines an H α bar but no SF activity is present in the galactic centre (archetype: NGC 3359).

Type B. Numerous H II regions are seen in the stellar bar and SF activity is present in the nuclear region (archetype: NGC 7479).

Type C. H II regions are few (or absent) and faint in the bar but intense SF activity is observed in the nuclear (or circumnuclear) region (archetype: NGC 3504).

From our sample, it is clear that the last type is observed mainly in early-type galaxies like NGC 3504 and NGC 5921

(see Table 1). However, our sample is too small to draw any firm conclusions concerning a possible trend between the Hubble type and the type of SF distribution in bars. Phillips (1996) and García-Barreto et al. (1996) showed that such a correlation exists in their larger samples. However, as a counter-example, a Type C distribution is observed in the massive SABc galaxy NGC 4303, a member of the Virgo Cluster (Martin & Roy 1992). In general, the H II regions of Type A are roughly distributed on a single axis but for some bars, like the ones in NGC 5068, NGC 4731 and NGC 7741, H II regions are also observed *outside* these H α bars. This is a significant result, suggesting that the gas clouds in these bars are not only concentrated along their major axis but are also present across the whole barred structure.

There is another important morphological property observed in a few objects studied here: *bars with strong dust lanes show a good correlation between the location of the H II regions and the dust lanes*. This is seen for instance in NGC 3504 where the small chains of H II regions seen in Fig. 1 are observed adjacent to the dust lanes. The bar of NGC 7479 is another example, its H II regions tracing the characteristic curved shape of strong dust lanes along bars (e.g. Athanassoula 1992). For a few objects small dust lanes roughly perpendicular to the bar can also be observed on the continuum images (particularly evident in NGC 3319, NGC 3359, NGC 3504, NGC 5068 and NGC 7479). However, contrary to the strong dust lanes, no obvious correlation seems to exist between these features and the H II regions. Additional data (e.g. BVI imaging) with better resolution are necessary to confirm these results.

3.2. Quantitative properties

To establish constraints for numerical simulations, characteristics of the H α bars have been studied quantitatively. First, considering the *stellar bars* as elliptical features, their projected semi-major axes a , semi-minor axes b , axial ratios b/a , and position angles have been measured on the continuum images using the ELLIPSE package in IRAF. No measurements of harmonics higher than $m = 2$ have been attempted since only a first-order comparison between stellar and H α bars is possible. Uncertainties on the position angles are estimated to be $\pm 2^\circ$; comparison with data from Phillips (1993) shows very good agreement ($\leq 2^\circ$) for the stellar bar position angles of galaxies common to both works. Similar measurements of these parameters for the H α bars were performed, but not with ELLIPSE, these structures being too irregular for the isophotes to be traceable using an automatic procedure. Instead, quantitative parameters were measured on the images by studying the isocontours of the H α bars and matching an elliptical “envelope” to them. The position angle of the H α bars was then estimated with the major axis defined from this “envelope”.

The measurements related to the stellar bars, i.e. the semi-major and semi-minor axes, were defined as in Martin (1995): a is the length from the galaxy centre to the sharp outer tip of the bar near the junction with the spiral arms, and b is measured perpendicular to a and includes the spheroidal component if present. When defined this way, the bar axial ratios estimated

are in good agreement ($\sim \pm 10\%$) with the more quantitative definition of bars (elliptical features defined by $(b/a)_{\max}$) given by Wozniak et al. (1995) and used in the analysis of our numerical simulations.

The deprojected values of the relative length of the bar with respect to the disc, $L_b(i)$, and the axis ratio $b/a(i)$, have been calculated using the equations given by Martin (1995):

$$L_b(i) = \frac{2a \left(\cos^2 \phi_a + \sec^2 i \sin^2 \phi_a \right)^{1/2}}{D_{25}} \quad (1)$$

$$b/a(i) = \frac{b}{a} \left[\frac{\cos^2 \phi_b + \sec^2 i \sin^2 \phi_b}{\cos^2 \phi_a + \sec^2 i \sin^2 \phi_a} \right]^{1/2} \quad (2)$$

where D_{25} is the diameter of the galaxy at a surface brightness of 25 mag arcsec $^{-2}$, and $\phi_{a,b}$ are the angles between the bar axes and the galaxy node lines (PA in Table 1). As discussed by Martin (1995) the uncertainties on these quantities are high ($\sim \pm 20\%$) due to simplistic assumptions concerning projection effects, errors on the inclination and position angle values, difficulties in deconvolving bars and bulges, quality of images, etc. For all these reasons, the values given in Table 3 differ slightly from the visual measurements performed on photographic plates by Martin (1995). But, in general, a reasonable agreement ($\lesssim 10 - 20\%$) is found for galaxies common to both works.

Results are summarized in Table 3. A first important property of some H α bars is well illustrated in this Table: *when a major axis can be defined for the H α bars, significant apparent misalignments (θ) can be observed between the H α bar and its stellar counterpart (up to 15°)*. These angular misalignments are apparent in Fig. 1, in particular for NGC 1087 and NGC 3359. A similar behaviour was noticed by Phillips (1996) for a few late-type galaxies of his sample. Deprojected misalignments, $\theta(i)$, were also calculated according to the formula:

$$\theta(i) = \arctan(\cos i \tan \phi_{a,\text{H}\alpha}) - \arctan(\cos i \tan \phi_{a,\text{S}}) \quad (3)$$

where $\phi_{a,\text{H}\alpha}$ and $\phi_{a,\text{S}}$ are the apparent angles between the major axes and the node lines for the H α bar and the stellar bar respectively. Values of $\theta(i)$ are given as the last entries for the H α bars in Table 3. In general, the corrections are small except for two objects (NGC 3359 and NGC 7741) where part of the large misalignment is attributable to projection effect. It is important to notice that the large misalignment values obtained for a few galaxies are still probably somewhat *underestimated* by a few degrees, since the ellipse fitting technique is affected by the convolution of the bright H II regions and the stellar continuum in these bars (“twisted” isophotes).

Except for one marginal case (NGC 7741, see next section), all the H α bars showing a misalignment are *leading* the stellar bar, if we postulate that the direction of rotation is given by the spiral arm structure assumed to be trailing. This assumption is confirmed for all the galaxies showing an angular misalignment and for which kinematic data (HI or ionized gas) are available (NGC 1073, NGC 3359, NGC 4731, NGC 7741).

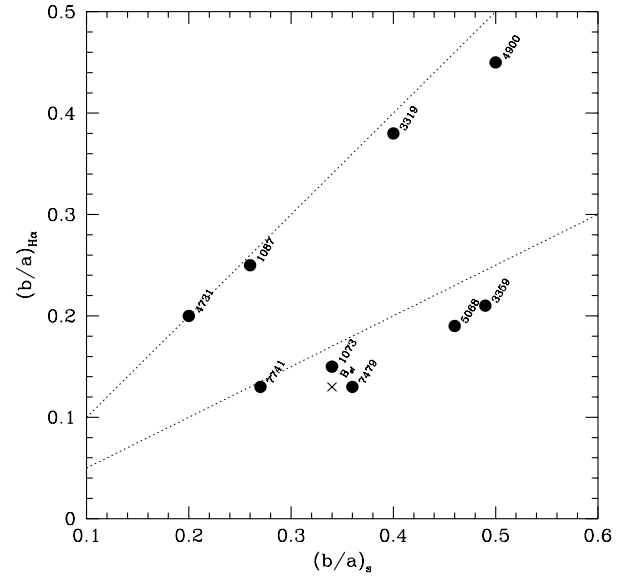


Fig. 2. Relation between the axis ratios for stellar bars, $(b/a)_S$, and for H α bars, $(b/a)_{\text{H}\alpha}$. Filled circles are galaxy Types A and B of Table 3 and the cross corresponds to the numerical model B_{SF} . Dotted curves have slopes 1.0 and 0.5 respectively

A close examination of Fig. 1 reveals also that *the H α bars can be considerably shorter than the stellar bars*. In Table 3 this property is quantified by the relative length of the bars with respect to the galactic disc. The deprojected length ratio between the H α bar and the stellar bar varies greatly in our sample, from ≈ 0.36 in NGC 7741 to ≈ 0.92 in NGC 5068. This morphology gives the impression of “gaps” at the ends of the bars since the H II regions are generally concentrated in their inner parts.

Finally, the axial ratios given in Table 3, show that in some cases *the H α bars can be much narrower than the stellar bars*. This is particularly obvious for NGC 3359 and NGC 5068 where the gas bars have deprojected axial ratios smaller by a factor of ≈ 2.3 and ≈ 2.4 than that of their stellar counterparts respectively. But the relation between stellar bar axis ratios and H α bar axis ratios for galaxy types A and B in Table 3 is more clearly seen in Fig. 2. There are two distinct groups of galaxies: in the first one, the axis ratios are similar whereas in the second group the H α bar axis ratios are more than twice smaller. However, since our galaxy sample is small, one should remain cautious before drawing conclusions. Indeed, we could simply have missed galaxies between these two groups. Another problem concerns inclination effects which could lead to overestimating $(b/a)_{\text{H}\alpha}$. Galaxies of the first group have the highest inclinations of the sample. Observed values in the numerical models are very close to those of the second group (see Sect. 5.3).

3.3. Notes on individual objects

Despite our general considerations on the morphology of SF activity along bars presented in Sect. 3.1, it is worthwhile examining the galaxies individually. Since interactions or mergers are possible causes of bar formation and of the subsequent SF

Table 3. Bar properties

Galaxy	Stellar bar					H α bar								Notes
	a ["]	b/a	$L_b(i)$	$b/a(i)$	PA [°]	Type	a ["]	b/a	$L_b(i)$	$b/a(i)$	PA [°]	θ [°]	$\theta(i)$ [°]	
NGC 1073	34	0.37	0.25	0.34	61	B	19	0.16	0.14	0.15	65	4	4	1
NGC 1087	9	0.36	0.16	0.26	126	B	9	0.26	0.14	0.25	139	13	12	2
NGC 3319	36	0.22	0.20	0.40	40	A	21	0.21	0.11	0.38	40	0	0	3
NGC 3359	31	0.35	0.16	0.49	12	A	24	0.17	0.14	0.21	27	15	10	4
NGC 3504	30	0.45	0.37	0.54	142	C	–	–	–	–	–	–	–	5
NGC 4731	30	0.18	0.28	0.20	127	B	24	0.18	0.22	0.20	126	1	1	6
NGC 4900	10	0.50	0.15	0.50	139	A	10	0.45	0.15	0.46	146	7	7	7
NGC 5068	25	0.45	0.12	0.46	151	A	22	0.18	0.11	0.19	147	4	4	8
NGC 5921	33	0.51	0.26	0.45	18	C	–	–	–	–	–	–	–	9
NGC 7479	52	0.27	0.44	0.36	9	B	34	0.10	0.29	0.13	9	0	0	10
NGC 7741	29	0.36	0.33	0.27	105	A	10	0.20	0.12	0.13	93	-12	-16	11

Notes

- (1) SF asymmetry in the bar; bar centre difficult to identify
- (2) Faint stellar bar; very significant misalignment; type uncertain
- (3) No misalignment; very symmetric SF along the bar; H α bar considerably shorter
- (4) Considerable misalignment; short dust lanes \perp to the bar
- (5) SF strongly correlated with dust lanes
- (6) Major axis of the H α bar difficult to identify
- (7) Stellar bar centre difficult to identify; strong misalignment
- (8) H α bar much narrower; faint stellar bar; some SF outside H α bar major axis; dust lanes \perp to the bar
- (9) Very faint H II regions in the bar; SF asymmetry in the bar
- (10) SF strongly correlated with strong dust lanes along the bar; faint dust lanes \perp to the bar
- (11) H α bar on one side of the stellar bar and apparently trailing; SF outside the major axis of the H α bar

activity in the bars (e.g. Noguchi 1988; Barnes & Hernquist 1991), it is important to review signatures for such events for these galaxies.

NGC 1073. There is a clear SF asymmetry in the bar with the two brightest H II regions located to the SW. A faint “bridge” appears between these regions but it could be an artifact of the continuum subtraction. The H II regions are confined to one axis. No SF enhancement is observed at the end of the stellar bar. Although there are no obvious companions near the galaxy (Martin & Roy 1994), England et al. (1990) found an asymmetry in the H I distribution and suggested that an interaction may have perturbed the galaxy in the recent past. Indeed, simulations of a strong interaction between a large galaxy and a small one by Noguchi (1988) revealed striking morphological similarities with NGC 1073. The central part of the galaxy is moderately gas-rich (Hunter & Gottesman 1996). Neither Kaufman & Contopoulos (1996) or England et al. (1990) mention the presence of inner Lindblad resonances (ILRs) in NGC 1073. The radial O/H gradient across the disc is shallow, suggesting strong radial gas flows (Martin & Roy 1994).

NGC 1087. The stellar bar is very short but shows a few bright H II regions. The disc has a very low surface brightness. The apparent misalignment between the H α bar and the stellar bar is large (13°). An asymmetry of SF between the N and S parts of the disc is observed. Even if the object appears close to another galaxy (NGC 1090), Blackman (1980) found that NGC 1087 is not interacting and should be considered isolated.

NGC 3319. The H II region distribution in the bar is almost perfectly symmetric with respect to the galaxy centre. No mis-

alignment is observed. There appears to be slight enhancement of SF at both ends of the bar. The central part of the galaxy is very gas-rich (Hunter & Gottesman 1996). According to Moore & Gottesman (1996), the H I distribution is asymmetric but the galaxy is isolated and does not show signs of interaction. There is some indication of a break in the radial O/H gradient of this galaxy (Zaritsky et al. 1994), suggesting that the bar may be young (Roy 1996).

NGC 3359. This is the best example of an H α bar. A spectacular chain of H II regions is observed in the southern part of the bar but only one bright region (the brightest of the whole galaxy) is present in the northern part. A large apparent misalignment of about 15° is observed. SF is completely absent in the galaxy nucleus but seems enhanced at the ends of the bar. NGC 3359 is an isolated object except for a small H I cloud observed in its vicinity (Ball 1986) and its bar is moderately gas-rich (Hunter & Gottesman 1996). Martin & Roy (1995) have estimated an age of 400 Myr for the bar. According to Duval & Monnet (1985) and Ball (1992), there are no ILRs in this galaxy.

NGC 3504. This is a typical case of SF distribution in the bar of an early-type spiral. A few “chains” of faint H II regions are observed next to the dust lanes and tremendous SF is present in the galaxy centre. An enhancement of SF is observed at the SE tip of the bar. There are no clear signs of SF in the northern part of the stellar bar. An extensive study of the nuclear starburst in NGC 3504 has been presented by Kenney et al. (1993); they concluded that the nuclear starburst is recent (< 100 Myr). The presence of H II regions along the bar suggests that some gas is still falling toward the nucleus. The galaxy is a member of a

small group but shows no obvious sign of interaction. Kenney et al. (1993) found two ILRs in this galaxy.

NGC 4731. This barred galaxy shows a very open spiral structure and a low surface brightness disc. SF is distributed in the whole (extremely narrow) stellar bar. A few HII regions are observed near the centre of the bar but the nucleus is very difficult to find. According to our definition for the circumnuclear region (CNR, see Sect. 4.2), we consider this galaxy to be Type B. This peculiar (open) spiral morphology indicates a strong interaction with the nearby elliptical galaxy NGC 4697 (Sandage & Bedke 1994). The central part of NGC 4731 is moderately gas-rich (Hunter & Gottesman 1996) and the disc shows significant non-circular gas motions (Gottesman et al. 1984).

NGC 4900. Very bright H II regions (among the brightest of the whole disc) form a short H α bar showing a clear misalignment with the stellar bar (7°). No SF seems to be present in the galaxy centre but the latter is particularly difficult to locate. NGC 4900 is a member of the Virgo Cluster but with no obvious sign of interaction. Warmels (1988) has shown that the inner disc (including the bar) is gas rich (no H I depletion hole).

NGC 5068. The H II regions in the stellar bar are unevenly distributed along the major axis but are also present in the entire stellar bar. The dust distribution in the bar is quite complex, with lanes crossing the bar perpendicularly. The stellar bar is much larger than the H α bar. The global O/H gradient across the galaxy appears relatively shallow (-0.046 dex kpc^{-1} ; Ryder 1995).

NGC 5921. This is another example of an early-type galaxy with some SF in its bar. Faint H II regions are seen near the southern end of the stellar bar and also west of the nucleus which shows intense SF activity. A SF enhancement is observed at both ends of the stellar bar. Pogge (1989) classifies the nucleus of NGC 5921 as a LINER.

NGC 7479. This is another spectacular case of SF along the dust lanes of a bar. There is also SF activity in the galaxy centre and maybe some enhancement at the end of the bar. A short “chain” of H II regions is observed in the southern part of the bar, quite similar to the distribution observed in NGC 3504. There is a strong morphological asymmetry between the main spiral arms of the galaxy (one is very sharp, the other rather flocculent). The large-scale H I distribution appears normal except for an S-shaped radio continuum feature along the bar (Laine & Gottesman 1996). There, molecular gas is abundant and exhibits peculiar kinematics (Laine & Gottesman 1996). These features could be explained by a recent merging although no companion is seen (Laine 1996). There seems to be no ILRs (Duval & Monnet 1985; Sempere et al. 1995; Laine 1996).

NGC 7741. This galaxy corresponds to a very special case of SF in a stellar bar. The chain of H II regions observed above the nucleus (represented by the geometrical centre of the ellipse defining the stellar bar since no bulge could be found) is located to one side of the stellar bar (see also Duval et al. 1991). The angle formed with the major axis of the latter gives the impression that the H α bar is trailing. A bright H II region is also observed under the bar, illustrating a case similar to NGC 5068 where SF is observed outside the major axis. Duval et al. (1991) found

strong gas flows in the bar region and a ratio of 30% between the bar mass and that of the inner disc inside the bar radius. No ILRs are present (Duval et al. (1991)).

4. Star formation rates

4.1. Procedure

As described by Kennicutt (1983), the absolute H α luminosity of H II regions, $L_{\text{H}\alpha}$, can be used to derive the total star formation rates in galaxies (see also Phillips 1993; Contini 1996). If the Miller-Scalo IMF, represented by $\psi(m) \propto m^{-\gamma}$ with $\gamma = 1.4$ for $0.1 < m < 1.0 M_\odot$ and $\gamma = 2.5$ for $1.0 < m < 100 M_\odot$, is adopted, the total SFR is given by:

$$\text{SFR}_{\text{tot}}(0.1 - 100 M_\odot) = \frac{L_{\text{H}\alpha}[\text{erg s}^{-1}]}{1.12 \cdot 10^{41}} [M_\odot \text{ yr}^{-1}] \quad (4)$$

with $\text{SFR}(> 10 M_\odot) = 0.16 \text{SFR}_{\text{tot}}$. The luminosity is defined by:

$$L_{\text{H}\alpha} = 4\pi D^2 f(\text{H}\alpha) 10^{0.4A(\text{H}\alpha)} (1 + L_\gamma)(1 + R_{[\text{N II}]})^{-1} \quad (5)$$

where D is the distance to the galaxy, $f(\text{H}\alpha)$ is the integrated H α flux in $\text{erg cm}^{-2} \text{ s}^{-1}$ ($f(\text{H}\alpha + [\text{N II}])$ if the [N II] lines are included), $A(\text{H}\alpha)$ is the total (galactic + extragalactic) extinction in H α , L_γ is the estimated fraction of Lyman photons escaping the nebula (photon leaking), and $R_{[\text{N II}]}$ is the [N II] λ 6548, 6584 to H α line ratio (if the [N II] lines are included). These last three parameters are discussed below.

The major uncertainty in this method is the correction for dust extinction. In his extensive study of spirals, Kennicutt (1983) favors $A(\text{H}\alpha) = 1.1$ magnitudes for the disc H II regions. More recent studies have confirmed this value (e.g. for NGC 2997, $\langle A(\text{H}\alpha) \rangle \sim 1.2$; Walsh & Roy 1989). However, for some galaxies, this value can be quite different (e.g. M101 with $\langle A(\text{H}\alpha) \rangle \sim 0.2$; Kennicutt & Garnett 1996). There are two important caveats in deriving such a value from optical data (e.g. H α /H β): 1) a very simplistic model of dust extinction is assumed; 2) the Balmer lines may be strongly affected by the underlying continuum extinction, resulting in possible overestimation of extinction (this is particularly true for many regions in bars as will be discussed in Paper II). To avoid the second difficulty the underlying absorption can be corrected by adding a few equivalent widths of continuum (cf. McCall et al. 1985) but this cannot be achieved if the absorption is too large (e.g. Oey & Kennicutt 1993). From our sample of spectra, we have selected a few H II regions along the bars of galaxies which do not show a strong underlying absorption and carefully studied their H α /H β ratios. Our analysis reveals that the average extinction for these H II regions (not the circumnuclear ones) is $\sim 1.0 \pm 0.3$ mag, in agreement with the average value stated above. Thus, we have also adopted 1.1 mag as the extinction affecting the H α fluxes of the H II regions in our sample of bars. For the circumnuclear H II regions, Phillips (1996) has argued that the real extinction is much higher, by at least 2 mag, than the value obtained from H α /H β . Therefore, for regions of this type, we have used $\langle A(\text{H}\alpha) \rangle = 3.0$ mag.

Authors of recent studies on nuclear starbursts and diffuse $H\alpha$ emission across galactic discs have suggested that a non-negligible fraction of ionizing photons could escape H II regions (Leitherer et al. 1996; Hoopes et al. 1996). If no correction is applied the SFRs are severely underestimated. According to Hoopes et al. (1996), 30% to 55% of the total $H\alpha$ emission from disc galaxies can be diffuse and not be directly associated with H II regions. The origin of this emission is still unclear but some of it probably comes from photons leaking from nebulae. As a conservative estimate, we will assume $L_\gamma = 0.25$ in our calculations of the SFRs.

Finally, another correction taking into account the contribution of the $[N II] \lambda 6548, 6583$ lines has to be applied to our $H\alpha$ fluxes for the galaxies observed with the larger bandpass (70 Å) $H\alpha$ filters. In a normal H II region, $R_{[N II]} \sim 0.33$ (e.g. McCall et al. 1985) but this ratio depends on the nebular conditions. In particular, if strong shocks or hard UV-radiation are present, $[N II]/H\alpha$ becomes much larger (Osterbrock 1989). This is the case for most of the circumnuclear H II regions (Osmer et al. 1974; Kennicutt et al. 1989) where $[N II]/H\alpha$ can be larger than 1. Based on the spectra obtained for a sub-sample of H II regions not located in the vicinity of the nuclei in the galaxies studied here, $[N II]/H\alpha$ varies considerably, from ~ 0.25 to 0.65 (Martin 1996; Paper II). Hence, instead of assuming a rough, constant, $[N II]/H\alpha$ ratio for all the galaxies affected, we have calculated an average $R_{[N II]}$ ratio observed in the bar of each individual object: NGC 1087 (0.43); NGC 3319 (0.31); NGC 3359 (0.38); NGC 3504 (0.63); NGC 4900 (0.36); NGC 5921 (0.51); NGC 7479 (0.48); NGC 7741 (0.36). An average $[N II]/H\alpha$ was also calculated for the circumnuclear regions. No correction was applied for the bars of the other galaxies of the sample. For galaxies where it was possible to calculate the SFR in their discs (and for which the $H\alpha$ flux was contaminated by the $[N II]$ lines), we assumed $R_{[N II]} = 0.33$.

In short, individual SFRs suffer from large uncertainties and differences of a factor of 2 or 3 between various studies are not surprising (see also Phillips 1993 and Martinet & Friedli 1997). Thus, although instructive, the following calculations should be considered with great caution.

4.2. SFR distributions

The star formation rates for various regions in each galaxy of our sample are given in Table 4: SFR_{bar} is the total rate of star formation from H II regions in the bar *excluding* nuclear and circumnuclear regions if present; SFR_{CNR} is the total star formation rate for the nuclear and circumnuclear regions (estimated from the $H\alpha$ integrated flux inside a radius $< 0.1a$, except for NGC 3504 where the strong starburst defines a circumnuclear region with a radius $\sim 0.25a$); SFR_{disc} is the total star formation rate in the disc region. We also define the star formation rate for the whole galaxy SFR_{gal} as well as $\beta = SFR_{\text{CNR}}/SFR_{\text{bar}}$. The values of SFR_{gal} were calculated only for the galaxies for which the *total* integrated $H\alpha$ flux was measurable on our CCD images.

For the other galaxies, the restricted field of view of our images does not allow estimates of SFR_{gal} .

The $H\alpha$ bar types introduced in Sect. 3.1 are now quantitatively defined: Type A has $\beta \leq 0.2$; Type B, $0.2 < \beta < 5.0$; and Type C, $\beta \geq 5.0$. Due to the small size of the sample, these limits are not definitive values and, at the moment, should only be considered as a quantitative representation of the SF morphologies found along galactic bars.

From these data the following results emerge: 1) when excluding the circumnuclear star formation activity, *SFR in bars cover a large range of values (variation by a factor of ~ 50)*; 2) the total SFR in the bar region generally accounts for a moderate fraction of the galaxy's total star formation ($\lesssim 30\%$); 3) the two galaxies presenting the strongest signs of a recent interaction or merging (NGC 4731 and NGC 7479) show the highest SFR in their bars; 4) there is no correlation between the radial position of the H II regions along the bar and their SFR, i.e. the intensity of SF is distributed randomly along the bar major axes.

Let us quantify the SF asymmetry observed in many bars. The amplitude of the SF asymmetry between both sides of the bar with respect to the minor axis is defined as:

$$\Delta_{\text{bar}} = \frac{|SFR_{\text{side1}} - SFR_{\text{side2}}|}{SFR_{\text{bar}}}. \quad (6)$$

For instance, $\Delta_{\text{bar}} = 0$ and 1 correspond to a very symmetric and a very asymmetric bar respectively. The values are given in the last column of Table 4. Again, a large range is observed (from 0.21 to 1.00). No clear trend is observed between the type of distribution and the amplitude of the SF asymmetry.

4.3. Application: the gas-to-star transformation efficiency in NGC 7479

One of the main problems related to the role played by bars in triggering nuclear starburst or AGN activity is estimating the fraction of gas funnelled along the bar that will actually reach the central region without being transformed into stars. The main difficulty is measuring the gas inflow rate along the bar. The absence of a good theory of star formation represents a severe limitation for the numerical simulations. Recently, Quillen et al. (1995) have suggested a method to derive from NIR images the gas mass inflow rates, dm_g/dt , by considering the gravitational torque exerted on the gas by the bar. In particular, for NGC 7479, they found $dm_g/dt = 4 \pm 2 M_\odot \text{ yr}^{-1}$. However, this value must be considered with great caution. The gravitational torque is a highly varying function of the radius and can change sign at each resonance, in particular at ILRs. Nevertheless, the value derived by Quillen et al. (1995) is consistent with what is observed in SPH (Smooth Particle Hydrodynamics) simulations of spontaneous bar formation (see Sect. 5.5). For instance, in NGC 7479, Laine (1996) found an inflow rate of $4.5 M_\odot \text{ yr}^{-1}$ in his SPH simulations. In models of minor galaxy mergers developing a strong bar in the main component (e.g. Mihos & Hernquist 1994), similar rates are observed. This value is higher than the inflow rate seen in hydrodynamic simulations with fixed stellar

Table 4. SFR distributions

Galaxy	SFR _{bar} ^a	SFR _{CNR} ^a	SFR _{disc} ^a	SFR _{bar} /SFR _{CNR} ^b	SFR _{bar} /SFR _{disc} ^b	SFR _{bar} /SFR _{gal} ^b	β	Δ_{bar}
NGC 1073	0.08	0.05	1.20	160	7	6	0.6	0.85
NGC 1087	0.12	0.18	1.31	67	9	8	1.5	0.50
NGC 3319	0.06	–	1.94	–	3	3	0.0	0.28
NGC 3359	0.37	–	1.81	–	20	17 ^c	0.0	0.28
NGC 3504	0.28	16.10	1.62	2	17	2	50.0	1.00
NGC 4731	1.44	3.31	4.00	44	36	17	2.3	0.56
NGC 4900	0.36	–	1.89	–	19	16	0.0	0.26
NGC 5068	0.03	–	0.35	–	9	8 ^d	0.0	0.21
NGC 5921	0.09	0.66	–	14	–	–	7.1	0.71
NGC 7479	0.40	0.63	–	64	–	–	1.6	0.23
NGC 7741	0.11	–	0.62	–	18	15	0.0	0.63

Notes: ^a in $M_{\odot} \text{ yr}^{-1}$; ^b in%; ^c from Martin & Roy (1995); ^d from Phillips (1993).

potentials performed by Athanassoula (1992). Hence the gas inflow rate in the bar of NGC 7479 derived by the above methods should be considered as an upper limit.

If we assume that both the inflow and the star formation rates are constant over a few Myr inside the bar, the gas-to-star transformation efficiency, $\eta = \text{SFR} / (\frac{dm_g}{dt})$, can be roughly estimated. According to the values given in Table 4, the transformation efficiency *along* the bar is $\eta_{\text{bar}} = 0.10$. This result suggests that *maybe as much as 90% of the gas flowing into the bar of NGC 7479 is not transformed into stars*. When reaching the centre, $\eta_{\text{CNR}} = 0.16$ according to Table 4; at most, about 26% of the gas falling in the bar region is consumed into stars at present time.

Is this last value severely underestimated? As mentioned above, dm_g/dt is an highly uncertain value and is probably an upper limit. However, the main uncertainty of the method is introduced by the absolute value derived for the SFR in the bar of NGC 7479. The presence of significant star formation in the central region of NGC 7479 indicates that at least some gas is falling into the centre i.e. $\eta_{\text{bar}} < 1.0$. Dust extinction could severely affect the derivation of the SFR, but the total SFR in the bar region ($\text{SFR}_{\text{bar}} + \text{SFR}_{\text{CNR}}$) may be overestimated for this object. Indeed, the spectra of the H II regions along the bar give $\langle A(\text{H}\alpha) \rangle \sim 0.8$ mag (we applied 1.1 mag) and we used 3.0 mag for the circumnuclear SF. Using $H_0 = 100$ for the distance scale would increase the total SFR by a factor of 1.8, i.e. $\eta = 0.45$. In short, it is likely that a large fraction of the gas sinking into the bar region, probably $> 50\%$, is not transformed into stars (this number is certainly higher for the gas funnelled along the bar). Numerical models give similar values (see Sect. 5.5 and Laine 1996). If one assumes that the inflow rate and the total gas-to-star transformation efficiency in the bar region are good approximations of the *average* values since the early-phase of the formation of the bar in NGC 7479 (considered to be about 500 Myr ago), a mass of gas of about $2 \cdot 10^9 M_{\odot}$ should be present in the galaxy centre. This is exactly the mass of molecular gas found in the *circumnuclear region* of NGC 7479 by Laine (1996).

The gas-to-star transformation efficiency can also be defined with respect to the mass of gas present in the bar (see Sect. 5.5). In NGC 7479, there is no neutral gas in the bar but molecular

gas is very abundant ($\sim 2 \cdot 10^9 M_{\odot}$ along the bar, $\sim 2 \cdot 10^9 M_{\odot}$ in the nuclear region; Laine 1996). In 10 Myr, only 0.2% of the gas along the bar is transformed into stars. This value differs by more than one order of magnitude from the previous method (10%)! Qualitatively however, the result is the same: most of the gas falling along the bar will sink into the galaxy centre. Numerical models give values between these two extremes ($\sim 1\%$; Sect. 5.5).

5. Numerical simulations

Within the framework of our new observational results, the self-consistent 3D numerical simulations of spontaneous bar formation described in FB95 are thoroughly re-analyzed, especially the fiducial model B_{sf} . The presentation of more extended and detailed numerical models with higher spatial resolutions is deferred to Paper III of this series. Here, the emphasis is on misalignments between stellar, gaseous, and H α bars as well as on the length and axis ratio characteristics of these different bars. In the numerical models, the H II regions have arbitrarily been defined as being all the new stars (i.e. the star particles generated by the star formation process) created within a period of 10 Myr previous to the analysis time.

The technical details of the numerical simulations as well as the description of the various methods and models studied can be found in the following papers: Pfenniger & Friedli (1993) discuss the computation of the gravitational forces with a particle-mesh method using a 3D polar grid; calculation of the pressure and viscous forces affecting the gas component are presented by Friedli & Benz (1993) using the SPH technique; and FB95 detail the computation of the radiative cooling, the star formation “recipe” (based on the Toomre’s criterion for gravitational instability of gaseous discs Q_g (Toomre 1964)) as well as the specifications of the different models.

As a typical example, Fig. 3 shows the strong bar-induced evolution of the surface density of stars, gas, and H II regions, projected in the three principal planes for the model B_{new} (Sect. 5.5).

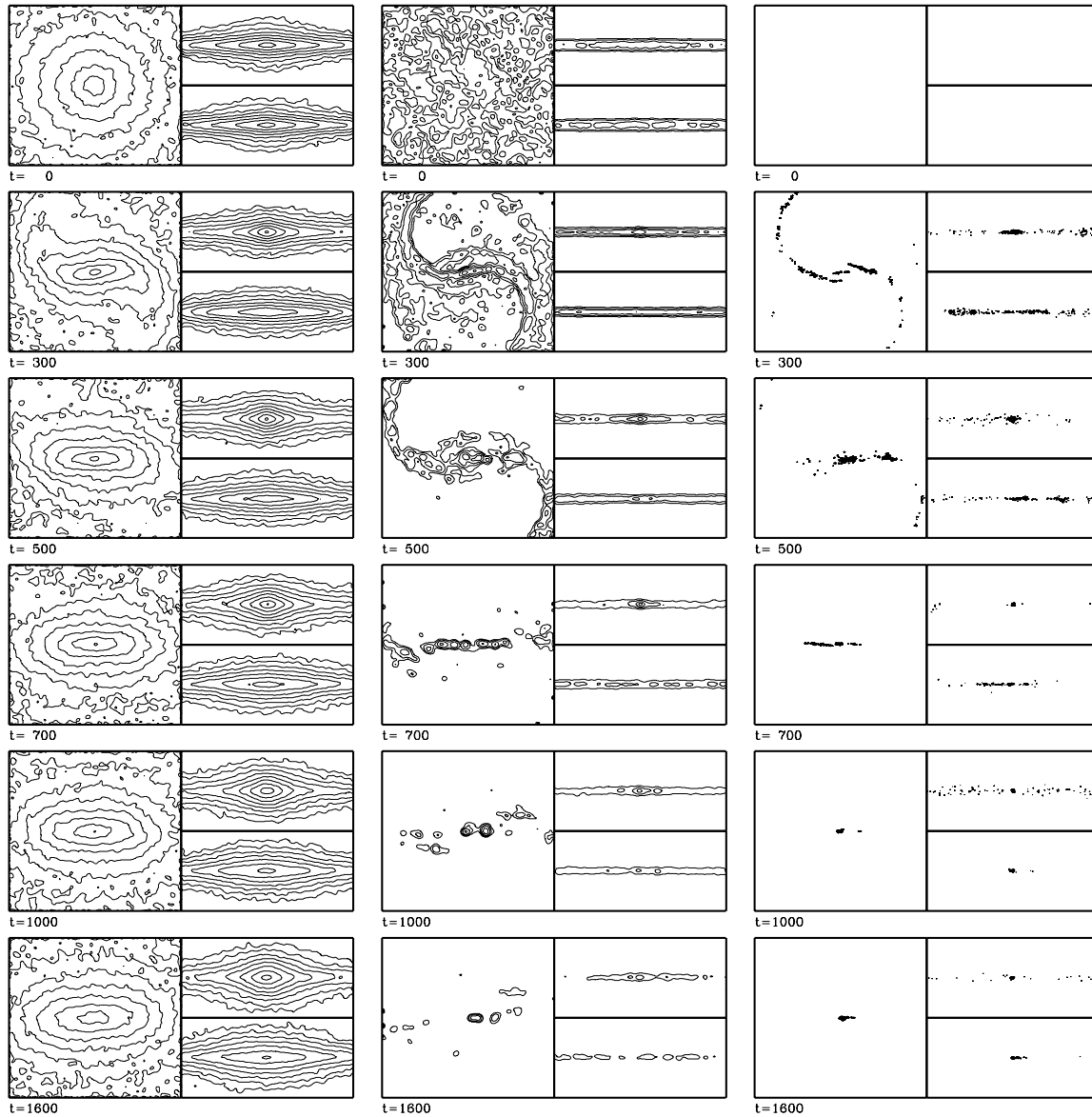


Fig. 3. Time evolution of the surface density projected in the three principal planes of the model B_{new} for the stars (left column), the gas (middle column), and the H II regions (right column). The side of the square frames is 16 kpc. The isodensity contours are separated by 0.3 dex. The time t is indicated at the bottom left of each frame in Myr. The stellar bar has horizontally been oriented and its rotation is counter-clockwise

5.1. Time-dependent systems: a word of caution!

The formation of a strong bar in an axisymmetric stellar disc is a highly non-linear, time-dependent phenomenon. The potential strongly evolves during the bar growth. Many bar parameters, if not all, are time variable on short time-scales, like the bar axis ratio $b/a = (b/a)(t)$, the bar pattern speed $\Omega_b = \Omega_b(t)$, etc. Numerical models only reach a quasi-stationary state after ≈ 10 bar rotations. If large amounts of gas are present in the system, the dissipation reinforces the time-dependent nature of the potential which will then never reach a quasi-stationary state in principle. In this context, the concept of resonances is of course poorly defined. As we shall see, several galaxies of the sample are supposed to have quite young bars and thus could well

personify highly time-dependent systems. In the following subsections, in order to make the discussion easier, we will often refer to the various bar parameters, the corotation (CR), and the ILRs, but these quantities should be considered with caution and regarded as purely indicative; at best, they might represent correct instantaneous values.

5.2. Stellar – H α bar misalignments

Several numerical models by FB95 reveal the existence of moderate misalignments between the different components similar to those observed. They occur mostly at early epochs during the formation of a strong, ILR-free, fast-rotating, bar. Let us focus on the generic numerical simulation B_{sf} . If by definition

the stellar bar is oriented so that its $PA=0^\circ$, then at $t=400$ Myr the gaseous bar in this model has $PA \approx +8^\circ$, whereas the H II regions have $PA \approx +5^\circ$. Both the gaseous and the H α bars *lead* the stellar bar but with a slightly different angle. Since the accuracy of the PA measurement is $\pm 1^\circ$, this 3° difference is significant. Note that the PA of the total potential is similar to that of the stellar bar; at this early time, the PA of the bar only made of all the newly formed stars is still similar to that of the H α bar.

The reason why the gaseous bar leads the stellar bar, i.e. is tipped ahead, is related to the fact that gas dissipates energy and loses angular momentum. Thus the gravitational torque caused by the stellar bar has to be negative. The H α bar is slightly less misaligned than the gaseous bar because it is made of non-dissipative particles (the new stars) which align very quickly (in a few tens of Myr) with the stellar bar.

The existence and amplitude of the misalignments could depend on many parameters: 1) star formation parameters such as the efficiency of star formation, the amount of mechanical energy injected, etc.; 2) stellar bar parameters like b/a , Ω_b , the radial surface density profile, the strength and extension of the ILRs, etc.; 3) gas parameters such as the level of viscosity, the sound speed c_s , the total gas-to-star mass ratio M_g/M_* , etc. If the influence of some of these parameters can easily be tested in self-consistent numerical simulations (e.g. M_g/M_*), the role of others is very difficult to check (e.g. Ω_b). Moreover, some of these parameters are not independent (e.g. the ILRs depend in an intricate way on b/a , Ω_b , and the density profile). Various possibilities are examined below.

Star formation parameters. The analysis of numerical simulations by FB95 indicates that the existence and amplitude of the misalignments do not seem to depend significantly on any star formation parameter. This is confirmed in Tables 3 and 4: no trend is observed between the angular misalignments and the total SFR in the bars.

Stellar bar parameters. Early hydrodynamic experiments by Sanders & Tubbs (1980) in fixed barred potentials revealed the possible misalignment of the gaseous and stellar bars provided that the CR is far beyond the bar end and an ILR is present. These authors found that when the pattern speed is progressively decreased, the misalignment between the two bars increases, finally reaching nearly 90° , with the gaseous bar leading the stellar one. Combes & Gérin (1985) also found a similar behaviour for their molecular bars. Combes & Elmegreen (1993) have suggested that early-type bars should rotate fast and end near CR, whereas late-type bars should rotate slowly and end well inside CR. However, the latter assertion remains very controversial (e.g. Sellwood 1996). Athanassoula (1992) performed an extended study of shock morphology in various fixed barred potentials and concluded that, in order to match observed dust lanes, the bar should end close to or slightly before the CR. In her study as in our simulations, many examples of offset or misaligned straight shocks are observed in the ILR-free, strongly barred models.

In summary, small misalignments of gaseous bars ($\lesssim 10^\circ$) are naturally produced in strong ($b/a \lesssim 0.6$), fast-rotating (CR $\approx a$), ILR-free stellar bars, whereas the presence of an ILR is certainly a prerequisite for larger misalignments of gaseous bars ($10^\circ \lesssim \theta \lesssim 90^\circ$) in possibly slowly rotating stellar bars.

Gas parameters. From the analysis of numerical simulations by FB95, no significant variations in the misalignment amplitude have been detected in the models having $M_g/M_* = 0.05, 0.10, 0.20$ respectively. Likewise similar misalignments are observed for sound speeds $c_s \approx 7, 15, 22$ km s $^{-1}$.

As has already been stated, the viscosity is essential for producing misalignments. When it is switched off, gas and stars have very similar dynamics and no misalignments occur. However, we were unable to highlight any difference in the misalignment amplitude when the viscosity was increased/decreased by a factor of two. An increase by a factor of ten results in such a high dissipation rate that all the gas flows very quickly to the centre and no gaseous bar even form! This problem certainly requires further investigations.

5.3. Stellar – H α bar axis ratios

The stellar bar axis ratios have been determined using standard ellipse fits (Wozniak et al. 1995), and by choosing the maximum value $(b/a)_{\max}$ since it is both accurately and unambiguously defined. The generic model B_{sf} at $t=400$ Myr has $(b/a)_S \approx 0.34$. The determination of the axis ratio of the H α bars is more problematic due to the clumpiness of the distribution. Ellipse fits generally do not work; we simply use the ratio between the length of the H α bar which is easily determined and its maximum width extension. For the generic model B_{sf} at $t=400$ Myr, $(b/a)_{\text{H}\alpha} \approx 0.13$. In numerical models forming a strong bar, the H α bar axis ratios, as well as the gaseous bar axis ratios, are much smaller than the stellar ones. The fiducial model is indicated by a cross in Fig. 2 and is very close to the position of both NGC 1073 and NGC 7479.

5.4. Stellar – H α bar lengths

The generic model B_{sf} at $t=400$ Myr has a stellar bar of total length of ≈ 14.0 kpc, whereas the H α bar is ≈ 5.2 kpc, which corresponds to a length ratio of about 0.37. Although significant gas mass remains near the end of the stellar bar, SF is suppressed there since the SF threshold has been reached. The above value falls close to the lower bound of the observed values, but for instance at $t=320$ Myr a much larger value (0.64) is found. This is closer to the observed values for NGC 1073 (0.56) and NGC 7479 (0.65). Thus, this quantity appears to be strongly time-dependent and connected to the SF threshold. As the bar starts to form, SF is present almost all along the bar major axis. As time goes on, less and less gas is found at the end of the bar and the H α bar becomes shorter and shorter with only a few sporadic modest bursts of SF at the bar outskirts.

Table 5. Influences on SFRs of parameter variation

Parameters	$SFR_{\text{bar}}/SFR_{\text{CNR}}$	$SFR_{\text{bar}}/SFR_{\text{disc}}$	$SFR_{\text{bar}}/SFR_{\text{gal}}$
Star formation efficiency ϵ	\searrow	\searrow	\rightarrow
Mechanical energy injected E_M	\searrow	\nearrow	\rightarrow
Q_g threshold λ	\searrow	\searrow	\nearrow

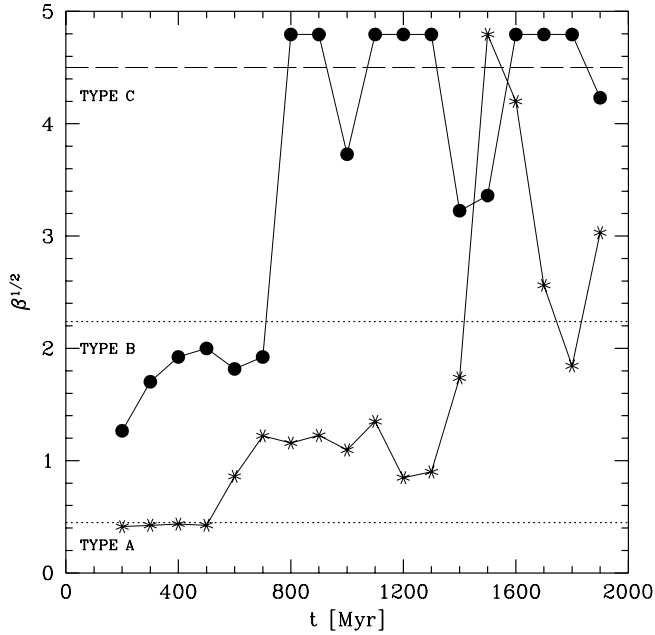


Fig. 4. Evolution of $\beta = SFR_{\text{CNR}}/SFR_{\text{bar}}$ in two different numerical simulations. Filled circles correspond to the fiducial model B_{sf} , and stars to model B_{new} . The square root of β has been plotted to compress the scale. Values of $\beta^{1/2}$ greater than 4.5 (dashed line) have arbitrarily been set to 4.8. Dotted curves separate regions of various types.

5.5. SFR distributions

Generalities. A thorough analysis of the SF properties in numerical models of barred galaxies can be found in FB95. In particular, the influence of the various star formation parameters has been investigated. Here, we specifically elaborate on the distribution and evolution of the SFR along the bar. It is mainly influenced by three parameters: the star formation efficiency ϵ , the amount of mechanical energy released in the interstellar medium E_M , and the Q_g threshold λ (new stars are formed if $Q_g < \lambda$). The variation of these parameters influences the relative level of SFR_{bar} with respect to the centre, disc, and total values as summarized in Table 5. Observed values from Table 4 constrain the possible values of the parameters involved in the numerical simulations. For instance the fact that $SFR_{\text{bar}}/SFR_{\text{CNR}} \approx 0.4 - 0.7$ for three Type B H α bars indicates that E_M cannot be zero and ϵ cannot be one in these galaxies. High values of E_M as well as low values of ϵ also have to be discarded.

SFR ratios. For the model B_{sf} , the peak SFR along the bar is $\approx 2 M_{\odot} \text{ yr}^{-1}$ at $t \approx 300$ Myr. This value appears to be much higher than what is generally observed in Table 4 (except for

NGC 4731). It is in fact not very useful to compare absolute SFR values since in numerical models they could easily be re-scaled for instance by changing the total gas mass of the system. It is more relevant to analyze dimensionless numbers like the SFR ratio β , or the gas-to-star transformation efficiencies η . The evolution of β with time is shown in Fig. 4. Around $t = 200$ Myr, $\beta \approx 1.5$, then it increases and remains $\approx 3 - 4$ from $t = 300$ Myr to $t = 700$ Myr. After that, β rapidly increases to more than 5 and remains very high until the end of the simulation at 2 Gyr. Therefore, this model starts as a Type B and then evolves towards a Type C. It never appears as a Type A. The ratios $SFR_{\text{bar}}/SFR_{\text{disc}}$ and $SFR_{\text{bar}}/SFR_{\text{gal}}$ are respectively 1.19 and 0.33 at $t = 300$ Myr, 1.26 and 0.21 at $t = 700$ Myr, and 0.09 and 0.02 at $t = 1$ Gyr.

With respect to the observations, the evolution of the generic model B_{sf} presents two serious issues: i) it never produces the Type A distribution of H II regions, i.e. the ratio $SFR_{\text{bar}}/SFR_{\text{CNR}}$ is too low; ii) the ratio $SFR_{\text{bar}}/SFR_{\text{disc}}$ is too high, especially at early times. Looking at Table 5, it is easy to see that a more adequate model should have a higher ϵ and/or a lower E_M , as well as a higher λ .

As a first step (see Paper III for the next ones), we have computed a model B_{new} similar to B_{sf} except that $\epsilon = 0.5$ (instead of 0.1), $\lambda = 1.8$ (1.4), and with 100 times less mechanical energy injected. The surface density evolution of this model is shown in Fig. 3 whereas the evolution of β is presented on Fig. 4, and the difference between both models is striking. Model B_{new} starts as a Type A (though nearly Type B), is a Type B between $t = 600$ Myr and $t = 1400$ Myr, and then seems to hesitate between Types B and C up to the end of the simulation at 2 Gyr. The ratios $SFR_{\text{bar}}/SFR_{\text{disc}}$ and $SFR_{\text{bar}}/SFR_{\text{gal}}$ are only slightly smaller than those for the fiducial model. Thus issue i) above is highly alleviated contrary to issue ii), i.e. this set of parameters seems not yet ideal! However, part of the problem might certainly be due the low gravitational resolution in the disc and at bar ends. Although large amounts of gas remain there, its concentration and its surface density are underestimated and consequently the SF is lower.

Asymmetries. At a given time in the numerical models, both sides of the bar have generally widely different SFRs. If the averaged value over a few hundreds of Myr only differs by a few percents, over a few tens of Myr the difference can be considerably higher. For instance, in both models, B_{sf} and B_{new} , Δ_{bar} (Eq. 6) takes nearly every value between ≈ 0.1 and ≈ 0.9 during the Type A and B phases. This is consistent with the observed values in Table 4. Thus, although at large scales of both time and length the SF distribution is essentially driven by the bar, at smaller scales stochastic processes start to dominate.

Gas-to-star transformation efficiencies. η_{bar} and η_{CNR} (see Sect. 4.3) have been estimated in the numerical models in different ways: $\eta_i = \tau \text{SFR}_i / M_{g,i}$ where $M_{g,i}$ is total gas mass in region i , $\tau = 10$ Myr, and $i = \text{bar}, \text{CNR}$. In model B_{sf} , η_{bar} is always very low, 0.01 or less, and η_{CNR} is higher. From about 0.15 at $t = 300$ Myr, it increases up to approximately 0.3 at $t = 600$ Myr, and then decreases progressively, reaching 0.1 at $t = 1$ Gyr. As expected in this model, the gas-to-star transformation appears very inefficient along the bar. During the Type B phase, the inferred η_{CNR} values tend to be higher than those found in Type B NGC 7479 (i.e. 0.16; see Sect. 4.3) whereas η_{bar} values are much smaller (0.10 for NGC 7479). This is another indication that model B_{sf} fails to reproduce various relevant observed quantities simultaneously. Things seem a little better in model B_{new} : indeed, η_{CNR} varies between 0.1 and 0.25, and η_{bar} always remains above 0.01 with a maximum value of 0.05 at $t = 600$ Myr.

5.6. ILRs

In model B_{new} , no ILRs are present during the first Gyr, then a weak (marginal) ILR appears up to the end of simulation at 2 Gyr. Both the progressive decrease of the bar pattern speed (30% from $t = 400$ Myr to $t = 1000$ Myr) and the slight 10% increase of the $\Omega - \kappa/2$ curve (due to central mass inflow) concur to produce this ILR. Thus, this resonance evolution suggests that H II distributions of Types A and B would occur in ILR-free bars whereas H II distributions of Type C would essentially appear in stellar bars with ILRs. The various mass models built for some galaxies in our sample also confirm this assertion (Sect. 3.3).

6. Conclusions

We have presented a study of H II regions located along the bar of eleven barred galaxies. A comparison with models from numerical simulations has been performed as well. Our main results are as follows:

- 1) Three main distributions are observed: H II regions along the bar only (Type A; 5 galaxies), H II regions in the bar and the galaxy nucleus (Type B; 4 galaxies), and strong star formation in the nuclear (or circumnuclear) region, but very weak or absent in the bar (Type C; 2 galaxies). ILRs seem to be absent in the barred galaxies with Types A and B contrary to those with Type C.
- 2) Numerical models suggest that the evolutionary trend is probably [Type A \rightarrow Type B \rightarrow Type C], although sporadic transitions from one type to another can also occur. Type A and B bars are thus considered to be young bars ($\lesssim 1$ Gyr). The type sequence observed in numerical bars (as well as the lifetime of a given type) crucially depends on some badly constrained star formation parameters, in particular the amount of mechanical energy released.
- 3) Numerical models with low (but non-zero) global mechanical energy release reproduce observations better.
- 4) In some galaxies, striking characteristics include a) angular misalignments (up to $\sim 15^\circ$) between the stellar bar and the

“H α bar”, b) much smaller axial ratios for H α bars than for the stellar ones, and c) much shorter H α bars than stellar ones. All these features have also been reproduced in our numerical models.

- 5) A correlation between the location of the H II regions and dust lanes in certain bars (mostly early-type spirals).
- 6) A wide range of SFRs (from 0.03 to $1.44 M_\odot \text{yr}^{-1}$) is observed in these H α bars. The ratio of the SFR along the bar to the SFR of the whole galaxy varies considerably from one galaxy to the other, between 0.02 and 0.17. In both observed and numerical galaxies, star formation is generally highly asymmetric with respect to bar minor axis.
- 7) The gas-to-star transformation efficiency in the bar of NGC 7479 is low (0.10), suggesting that perhaps as much as 90% of the gas funnelled along the bar is not transformed into stars and reaches the galaxy centre. This is confirmed by the large mass of molecular gas present in the circumnuclear region of this galaxy. All numerical models show low gas-to-star transformation efficiency in the bar region as well ($< 5\%$).

This work represents a first step to understand SF along galactic bars, but at least two important questions related to the morphology and SFR remain unanswered: 1) what is the fraction of bars showing SF for each Hubble type? 2) How do the luminosity functions of H II regions along bars differ from those of disc H II regions?

It is clear that the first question can only be answered by studying a very large sample of H α images of barred spirals along the Hubble sequence. This should not only help define the role of gas mass transfer across galactic discs by bars but it should also provide more constraints for the inflow rate and time evolution in numerical models. Indeed, the main theoretical issue concerns the way star formation parameters of the numerical models could be better constrained. Better statistics will help greatly.

The second issue is also important in order to follow the gas-to-stars transformation process in an environment where gas kinematics are strongly perturbed. High-resolution images would be extremely valuable in investigating this problem. Another point, as discussed earlier, is the difficulty of estimating the correct SFRs along bars due to dust extinction. Observations in the IR would be helpful as well. More kinematic data to derive the inflow rates and better constrained models should also result in an improved understanding of star formation processes and mechanisms for gas fueling AGN triggered by bars.

Acknowledgements. Discussions with S. Laine, L. Martinet and J.-R. Roy were most helpful. We thank R. Kennicutt for graciously providing the H α image of NGC 3319, M. Normandeau for having improved the English, and the referee, F. Combes, for her useful comments. We acknowledge the support offered by the technical staff of Mt-Mégantic Observatory and the Steward Bok Telescope. P.M. was supported by NSERC (Canada), FCAR (Quebec), and ESO postdoc fellowships during this work, and in part by the NSF through grant AST-94-21145. D.F. was supported by the University of Geneva (Geneva Observatory) and the Swiss National Science Foundation (FNRS) through an “Advanced Researcher” fellowship.

References

- Arsenault R., 1989, *A&A* 217, 66
- Athanassoula E., 1992, *MNRAS* 259, 345
- Athanassoula E., 1994, in: *Mass-Transfer Induced Activity in Galaxies*, Shlosman I. (ed.), Cambridge Univ. Press, Cambridge, p.143
- Ball R., 1986, *ApJ* 307, 453
- Ball R., 1992, *ApJ* 395, 418
- Barnes J.E., Hernquist L.E., 1991, *ApJ* 370, L65
- Blackman C.P. 1980, *MNRAS* 190, 459
- Combes F., Gérin M., 1985, *A&A* 150, 327
- Combes F., Elmegreen B.G., 1993, *A&A* 271, 391
- Contini T., 1996, Ph.D Thesis, Université Paul Sabatier, France
- de Vaucouleurs G., de Vaucouleurs A., Corwin H.G. Jr., et al., 1991, *Third Reference Catalogue of Bright Galaxies*, Springer Verlag, New-York
- Duval M.F., Monnet G., 1985, *A&AS* 61, 141
- Duval M.F., Monnet G., Boulesteix J., et al., 1991, *A&A* 241, 375
- England M.N., Gottesman S.T., Hunter J.H., 1990, *ApJ* 348, 456
- Englmaier P., Gerhard O., 1997, *MNRAS* 297, 57
- Friedli D., Benz W., 1993, *A&A* 268, 65
- Friedli D., Benz W., 1995, *A&A* 301, 649 (FB95)
- Friedli D., Benz W., Kennicutt R.C., 1994, *ApJ* 430, L105
- García-Barreto J.A., Franco J., Carrillo R., Venegas S., Escalante-Ramírez B., 1996, *Rev. Mex. Astron. Astrof.* 32, 89
- Gottesman S.T., Ball R., Hunter J.H., Huntley J.M., 1984 *ApJ* 286, 471
- Hawarden T.G., Mountain C.M., Leggett S.K., Puxley P.J., 1986, *MNRAS* 221, 41p
- Heller C.H., Shlosman I., 1994, *ApJ* 424, 84
- Hoopes C.G., Walterbos R.A., Greenawalt B.E., 1996, *AJ* 112, 1429
- Hunter J.H., Gottesman S.T., 1996, in: *Barred Galaxies*, IAU Coll. No. 157, Buta R., Elmegreen B., Crocker D. (eds.), ASP, San Francisco, p.398
- Isobe T., Feigelson E.D., 1992, *ApJS* 79, 197
- Jörsäter S., van Moorsel G.A., 1995, *AJ* 110, 2037
- Kaufmann, D.E., Contopoulos, G., 1996, *A&A* 309, 381
- Keel W.C., 1983, *ApJS* 52, 229
- Kennedy J.D.P., Carlstrom J.E., Young J.S., 1993, *ApJ* 418, 687
- Kennicutt R.C., 1983, *ApJ* 272, 54
- Kennicutt R.C., 1994, in: *Mass-Transfer Induced Activity in Galaxies*, Shlosman I. (ed.), Cambridge Univ. Press, Cambridge, p.131
- Kennicutt R.C., Garnett D.R., 1996, *ApJ* 456, 504
- Kennicutt R.C., Keel W.C., Blaha C.A., 1989, *AJ* 97, 1022
- Koopmann R.A., Kenney J.D.P., 1996, in: *Barred Galaxies*, IAU Coll. No. 157, Buta R., Elmegreen B., Crocker D. (eds.), ASP, San Francisco, p.105
- Laine S., 1996, Ph.D Thesis, University of Florida, USA
- Laine S., Gottesman S.T., 1996, in: *Barred Galaxies*, IAU Coll. No. 157, Buta R., Elmegreen B., Crocker D. (eds.), ASP, San Francisco, p.495
- Leitherer C., Vacca W.D., Conti P.S., et al., 1996, *ApJ* 465, 717
- Lindblad P.O., Hjelm M., Hoegbom J., et al., 1996, *A&AS* 120, 403
- Martin P., 1992, Ph.D Thesis, Université Laval, Canada
- Martin P., 1995, *AJ* 109, 2428
- Martin P., 1996, in: *Barred Galaxies*, IAU Coll. No. 157, Buta R., Elmegreen B., Crocker D. (eds.), ASP, San Francisco, p.70
- Martin P., Roy J.-R., 1992, *ApJ* 397, 463
- Martin P., Roy J.-R., 1994, *ApJ* 424, 599
- Martin P., Roy J.-R., 1995, *ApJ* 445, 161
- Martinet L., 1995, *Fund. Cosmic Physics* 15, 341
- Martinet L., Friedli D., 1997, *A&A* (in press)
- McCall M.L., Rybski P.M., Shield G.A., 1985, *ApJS* 57, 1
- Mihos J.C., Hernquist L.E., 1994, *ApJ* 425, L13
- Moore E.M., Gottesman S.T., 1995, *ApJ*, 447, 159
- Moore E.M., Gottesman S.T., 1996, in: *Barred Galaxies*, IAU Coll. No. 157, Buta R., Elmegreen B., Crocker D. (eds.), ASP, San Francisco, p.498
- Noguchi M., 1988, *A&A* 203, 259
- Oey M.S., Kennicutt R.C., 1993, *ApJ* 411, 137
- Ondrechen M.P., Van der Hulst J.M., 1989, *ApJ* 342, 290
- Osmer P.S., Smith M.G., Weedman D., 1974, *ApJ* 192, 297
- Osterbrock D.E., 1989, *Astrophysics of Gaseous Nebulae and Active Galactic Nuclei* (Mill Valley, CA: University Science Books)
- Piner B.G., Stone J.M., Teuben P.J., 1995, *ApJ* 449, 508
- Pfenniger D., Friedli D., 1993, *A&A* 270, 561
- Phillips A.C., 1993, Ph.D. Thesis, University of Washington, USA
- Phillips A.C., 1996, in: *Barred Galaxies*, IAU Coll. No. 157, Buta R., Elmegreen B., Crocker D. (eds.), ASP, San Francisco, p.44
- Pogge R.W., 1989, *ApJS* 71, 433
- Pompea S.M., Rieke G.H., 1990, *ApJ* 356, 416
- Quillen A.C., Frogel J.A., Kenney J.D., Pogge R.W., DePoy D.L., 1995, *ApJ* 441, 549
- Roberts W.W., Huntley J.M., van Albada G.D., 1979, *ApJ* 233, 67
- Roy J.-R., 1996, in: *Barred Galaxies*, IAU Coll. No. 157, Buta R., Elmegreen B., Crocker D. (eds.), ASP, San Francisco, p.63
- Ryder S.D., 1995, *ApJ* 444, 610
- Sandage A., Bedke, J., 1994, *The Carnegie Atlas of Galaxies*, (Washington: Carnegie Institution of Washington)
- Sanders R.H., Tubbs A.D., 1980, *ApJ* 235, 803
- Sellwood J.A., 1996, in: *Barred Galaxies*, IAU Coll. No. 157, Buta R., Elmegreen B., Crocker D. (eds.), ASP, San Francisco, p.259
- Sellwood J., Wilkinson A., 1993, *Rep. Prog. Phys.* 56, 173
- Sempere M.J., Combes F., Casoli F., 1995, *A&A* 299, 371
- Toomre A., 1964, *ApJ* 139, 1217
- Tully R.B., 1988, *Nearby Galaxies Catalog*, Cambridge Univ. Press, Cambridge
- Wada K., Habe A., 1992, *MNRAS* 258, 82
- Wada K., Habe A., 1995, *MNRAS* 277, 433
- Walsh J.R., Roy J.-R., 1989, *ApJ* 341, 722.
- Warmels R.H., 1988, *A&AS* 72, 57
- Wozniak H., Friedli D., Martinet L., Martin P., Bratschi P., 1995, *A&AS* 111, 115
- Wray J.D., 1988, *The Color Atlas of Galaxies*, Cambridge Univ. Press, Cambridge
- Zaritsky D., Kennicutt R.C., Huchra J.P., 1994, *ApJ* 420, 87